

Biochemistry. Author manuscript; available in PMC 2010 August 11.

Published in final edited form as:

Biochemistry. 2009 August 11; 48(31): 7411-7419. doi:10.1021/bi900535j.

NMR Structure and Dynamics of the Engineered Fluorescein-Binding Lipocalin FluA Reveals Rigidification of β -Barrel and Variable Loops upon Enthalpy-Driven Ligand Binding

Jeffrey L. Mills¹, Gaohua Liu^{1,3}, Arne Skerra^{2,*}, and Thomas Szyperski^{1,*}
¹Department of Chemistry, The State University of New York at Buffalo, Buffalo, NY 14260, USA

²Munich Center for Integrated Protein Science, CIPS-M, and Lehrstuhl für Biologische Chemie, Technische Universität München, Freising-Weihenstephan, Germany

Abstract

The NMR structure of the 21 kDa lipocalin FluA, which was previously obtained by combinatorial design, elucidates a reshaped binding site specific for the dye fluorescein resulting from 21 side chain replacements with respect to the parental lipocalin, the naturally occurring bilin-binding protein (BBP). As expected, FluA exhibits the lipocalin fold of BBP, comprising eight antiparallel β -strands forming a β -barrel with an α -helix attached to its side. Comparison of the NMR structure of the free FluA with the X-ray structures of BBP•biliverdin IX_γ and FluA•fluorescein complexes revealed significant conformational changes in the binding pocket, which is formed by four loops at the open end of the β-barrel as well as adjoining β-strand segments. An 'induced fit' became apparent for the side-chain conformations of Arg 88 and Phe 99, which contact the bound fluorescein in the complex and undergo concerted rearrangement upon ligand binding. Moreover, slower internal motional modes of the polypeptide backbone were identified by measuring transverse ¹⁵N backbone spin relaxation times in the rotating frame for the free FluA and also the FluA•fluorescein complex. A reduction of such motions was detected upon complex formation, indicating rigidification of the protein structure and loss of conformational entropy. This hypothesis was confirmed by isothermal titration calorimetry, showing that ligand binding is enthalpy driven, thus overcompensating negative entropy associated with both ligand binding per se and rigidification of the protein. Our investigation of the solution structure and dynamics as well as thermodynamics of lipocalin-ligand interaction does not only provide insight into the general mechanism of small molecule accommodation in the deep and narrow cavity of this abundant class of proteins but will also support the future design of corresponding binding proteins with novel specificities, so-called "anticalins".

Keywords

anticalin; bilin-binding protein; ligand binding; lipocalin; protein engineering

Lipocalins are globular proteins that occur in many organisms and serve primarily to store and transport poorly soluble or chemically sensitive metabolites(1). Although their pairwise

³Present address: Center for Advanced Biotechnology and Medicine, 679 Hoes Lane, Piscataway, NJ 08854, USA

^{*}Corresponding authors: AS, skerra@wzw.tum.de, T: +49 8161 71-4351 F: +49 8161 71-4352; TS, szypersk@buffalo.edu. **SUPPLEMENTAL INFORMATION:** 15 N spin relaxation times (T_1 , $T_{1\rho\text{-CPMG}}$, and $T_{1\rho\text{-CW}}$), heteronuclear 15 N{ 1 H}NOEs, and order parameters (S^2) for both FluA(R95K) and also for the FluA(R95K)•fluorescein complex may be accessed as supplemental materials free of charge online at http://pubs.acs.org

sequence homology is low (usually only 10-20%), lipocalins share a common fold comprising an eight-stranded antiparallel β -barrel with an attached α -helix (Figure 1). On one end, the β -barrel is "closed" by short loops and densely packed side chains that form the hydrophobic core. On the other end, the β -barrel is usually "open" to the solvent: there, four loops connecting neighboring β -strands form the entrance to the ligand-binding site. Whereas the β -barrel structure is strictly conserved among lipocalins, the loops around the ligand pocket are highly variable regarding length, amino acid sequence and backbone conformation(2). This finding provides a rationale for the diversity of binding specificities observed for this protein family in nature. In this respect, lipocalins may be compared with immunoglobulins, which carry a set of six structurally hypervariable loops on top of a rigid β -sheet sandwich, thus giving rise to a vast repertoire of antigen specificities(3).

Based on this notion, the lipocalin scaffold was chosen for engineering of artificial binding proteins with prescribed ligand specificities, so-called "anticalins" (2,4). In a first paradigmatic protein design effort, the binding pocket of the bilin-binding protein (BBP) from *Pieris brassicae*(5) was reshaped to recognize fluorescein(6), a well characterized immunological hapten(7) with many applications in the biological sciences(8). To this end, a combinatorial protein library was prepared by subjecting 16 amino acid positions (plus five additional fixed amino acid exchanges facilitating cloning and bacterial expression) spread across the four loops to simultaneous random mutagenesis, followed by phage display selection against the immobilized target compound. Thus, several hapten-specific BBP variants were obtained, including the anticalin FluA (carrying the amino acid substitutions N1D, N21Q, N34S, S35P, V36N, E37G, N58R, H60D, I69M, K87S, L88R, Y90V, V93Y, K95R, E96K, N97T, Y114S, K116R, Q125W, F127H, K135M), which exhibits high affinity and specificity for the free fluorescein ligand, characterized by a dissociation constant of K_D = 35 nM(6).

Engineered lipocalins that bind ligands other than fluorescein were subsequently selected from the same BBP random library, including an anticalin named DigA16, which recognizes with high affinity the hydrophilic plant steroid digoxigenin(9). Crystallographic analyses were conducted for FluA in complex with fluorescein(10) and also for DigA16 both as apoprotein and in complex with the ligands digoxigenin and digitoxigenin(10,11). These structural studies revealed that the lipocalin fold was retained in spite of the large number of side chain exchanges while considerable structural deviations from the natural BBP were detected in the loop regions, thus leading to the novel binding specificities. Notably, comparison of the X-ray structures of DigA16 and the two DigA16•ligand complexes(11) showed that the loop conformations were essentially unchanged in this case, indicating that the broad ligand-binding activity of lipocalins does not necessarily arise from dynamic flexibility of the loops at the open end of the β-barrel. However, this situation may be different for other lipocalins, whether natural or engineered. For example, several loops that are part of the binding pocket were found to be disordered in the crystal structure of the ligand-free human tear lipocalin (Tlc), indicating elevated flexibility(12). Also, conformational adjustments were observed in several structural studies of β -lactoglobulin, a well characterized lipocalin from cow milk, and its complexes with fatty acids and retinoids(13).

Indeed, the role of internal motional modes for ligand recognition by lipocalins is of particular interest with two different aspects: First, the ligand is often deeply buried within the β -barrel so that its accommodation apparently requires transient conformational rearrangements of large amplitude. This situation holds both for natural lipocalins such as the human retinol-binding protein (RBP)(14) and for engineered anticalins such as DigA16(11) and FluA(10) wherein just a narrow channel permits entry to the occluded ligand cavity. Second, some lipocalins are highly specific for their cognate ligands (*e.g.*,

RBP and BBP), whereas others (*e.g.*, Tlc) show promiscuity in their interaction with structurally diverse low molecular weight compounds. The latter may possibly correlate with an enhanced flexibility in the loop region, enabling a wider range of induced fit modes.

FluA(R95K), a variant of FluA carrying a back mutation at residue 95 (> 7 Å apart from the bound ligand) that leads to particularly high yield of functional protein upon bacterial periplasmic expression without measurably affecting the fluorescein-binding behavior(6), represents a paradigm lipocalin to investigate structural and functional dynamics by NMR. Whereas diffraction quality crystals of the uncomplexed protein were thus far not obtained, $\sim\!0.7$ mM solutions of FluA are stable for weeks. This enables the collection of all data required for a high-quality NMR structure determination. Moreover, an efficient *E. coli* expression system allows production of large quantities of stable isotope-labeled protein(15). Here we present (i) the high-quality NMR structure of FluA(R95K), (ii) its comparison with the X-ray structures of the FluA•fluorescein and BBP•biliverdin IX $_{\gamma}$ complexes, (iii) an investigation of slower internal motional modes based on measurement of 15 N spin relaxation times in the rotating frame for FluA(R95K) as well as for its fluorescein complex, and (iv) an isothermal titration calorimetric (ITC) study of the thermodynamics of fluorescein binding.

Materials and Methods

NMR Sample Preparation

NMR samples of stable isotope labelled 184-residue (21 kDa) FluA(R95K), including the C-terminal *Strep*-tag II (16) to facilitate protein purification, were produced as described(15). In addition, a biosynthetically directed fractional ¹³C-labeled sample(17,18) was generated for stereo-specific assignment of Val and Leu methyl groups. NMR samples of the FluA(R95K)•fluorescein complex were prepared by titrating solutions of *U*-¹³C, ¹⁵N-FluA(R95K) (for resonance assignment) or 50% ²H, *U*-¹⁵N-FluA(R95K) (for measurement of ¹⁵N spin-relaxation parameters) in NMR buffer (150 mM NaCl, 0.2 mM EDTA, 50 mM benzamidine, 10 mM Na-PO₄, pH 6.4) with fluorescein disodium salt (Sigma, MO) dissolved at ~1 mM concentration in the same buffer. Titration progress was monitored by recording 2D [¹⁵N, ¹H]-HSQC spectra(19) (Figure 1) and was in agreement with the expected 1:1 stoichiometry of ligand binding. Subsequently, the solution of the complex was concentrated to about 0.7 mM by use of YM-3 minicon centrifugal concentrators (Millipore, MA).

NMR Spectroscopy for Structure Determination of FluA(R95K)

Chemical shifts of FluA(R95K) were assigned as described(15). To derive conformational constraints for structure determination, spectra were recorded at 25 °C on Varian INOVA spectrometers equipped with conventional $^1H\{^{13}C,^{15}N\}$ triple resonance probes and operating at 1H resonance frequencies of 600, 750 or 900 MHz. NOE peak intensities were measured in the following spectra(19): (i) 2D [1H, 1H]-NOESY recorded for unlabeled FluA(R95K) in 90%/10% $H_2O/^2H_2O$ at 900 MHz, (ii) 2D [1H, 1H]-NOESY recorded for unlabeled FluA(R95K) in 100% 2H_2O at 900 MHz, (iii) 3D aliphatic ^{13}C -resolved [1H, 1H]-NOESY recorded for $U^{-13}C$, ^{15}N -labeled FluA(R95K) in 90%/10% $H_2O/^2H_2O$ at 750 MHz, (iv) 3D aliphatic ^{13}C -resolved [1H , 1H]-NOESY recorded for $U^{-13}C$, ^{15}N -labeled FluA(R95K) in 100% 2H_2O at 750 MHz, (v) 3D aromatic ^{13}C -resolved [1H , 1H]-NOESY recorded for $U^{-13}C$, ^{15}N -labeled FluA(R95K) in 100% 2H_2O at 750 MHz, (vi) 3D ^{15}N -resolved [1H, 1H]-NOESY recorded for $U^{-13}C$, ^{15}N -labeled FluA(R95K) in 90%/10% $H_2O/^2H_2O$ at 750 MHz, and (vii) 3D ^{15}N -resolved [1H , 1H]-NOESY recorded for 50% 2H , $U^{-15}N$ -labeled FluA(R95K) in 90%/10% $H_2O/^2H_2O$ at 900 MHz. NOESY data acquisition was complemented by recording 3D HNNHA(20) for measuring

backbone ${}^3J_{\mathrm{HN}\alpha}$ scalar couplings. The programs PROSA(21) and XEASY(22) were used for data processing and spectral analysis, respectively.

Structure Calculations of FluA(R95K)

NOE cross-peak volumes and ${}^3J_{HN\alpha}$ scalar couplings were converted, respectively, into ${}^1H^{-1}H$ upper distance limit and ϕ angle constraints using the program DYANA(23). Additional ϕ -and Ψ -angle constraints were derived from chemical shifts for residues located in regular secondary structure elements using the program TALOS(24). The final DYANA structure calculation employing torsion angle dynamics was started with 100 random conformers and 30,000 annealing steps. The 20 structures with the lowest target functions were selected to represent the NMR solution structure. R.m.s.d. values were calculated using the program MOLMOL(25). The coordinates were deposited in the Protein Data Bank (accession code 1T0V)

NMR Spectroscopy for Resonance Assignment of the FluA(R95K)•fluorescein Complex

For the ¹³C, ¹⁵N-labeled FluA(R95K)•fluorescein complex, 3D HNNCO(26), HNNCA(26), HNN(CO)CA(26), HNNCACB(27) and HNN(CO)CACB(28) were acquired for sequential polypeptide backbone and ¹³C^β resonance assignment. These backbone resonance assignments were required to measure backbone ¹⁵N spin relaxation parameters. The chemical shifts were deposited in the BioMagResBank (Accession code: 6182).

Measurement of Backbone ¹⁵N Spin Relaxation Parameters

Longitudinal backbone 15 N spin relaxation times $T_1(29)$, transverse 15 N spin relaxation times in the rotating frame - *i.e.*, Carr-Purcell-Meiboom-Gill $T_{1\rho\text{-CPMG}}(29,30)$ and continuous-wave (CW) spin-lock $T_{1\rho\text{-CW}}(31)$ – as well as steady-state heteronuclear 15 N{ 1 H}-NOEs(29) were recorded at 600 MHz 1 H resonance frequency for 50% 2 H,U- 15 N FluA(R95K) and for the 50% 2 H,U- 15 N FluA(R95K)•fluorescein complex. Cross-correlation between dipole-dipole and chemical shift anisotropy relaxation was suppressed by employing 180° 1 H pulses during the relaxation delays(32,33). All spectra were recorded with $t_{1,\max}(^{15}$ N) = 60 ms and $t_{2,\max}(^{1}$ H) = 64 ms.

 T_1 -relaxation times were determined from a series of 12 spectra recorded with relaxation delays of 5 (2×), 55, 130, 231, 341, 481 (2×), 742, 1063 (2×) and 1504 ms. $T_{1\rho\text{-CPMG}}$ -relaxation times were determined from a series of 12 spectra recorded with relaxation delays of: 8, 24 (3×), 32, 48 (2×), 64, 80, 88 (2×) and 104 ms. A long delay of 900 μ s was chosen between the 15 N 180° pulses of the CPMG train, so that most of the slow internal motional modes are not refocused. $T_{1\rho\text{-CW}}$ relaxation times were determined from a series of 12 [15 N, 1 H]-HSQC spectra recorded with relaxation delays of: 8, 24 (2×), 28, 36, 52 (2×), 64, 80, 92 (2×), and 108 ms. The 15 N CW spin-lock frequency was set close to the maximal experimentally feasible value, $\omega_{1,\text{CW}} = 28,050 \text{ rad} \cdot \text{s}^{-1}$. Hence, conformational exchange processes characterized by a correlation time $\tau_{\text{ex}} > \sim 1/\omega_{1,\text{cw}} = 35 \,\mu\text{s}$ or slower are largely refocused so that comparison of $T_{1\rho\text{-CPMG}}$ and $T_{1\rho\text{-CW}}$ relaxation times allows identification of slow internal motional modes. Steady-state 15 N{ 1 H}-NOE values were obtained from ratios of signal intensities registered in spectra recorded with either 5.0 s relaxation delay, or 1.5 s relaxation delay followed by a 3.5 s 1 H saturation period.

Analysis of Backbone ¹⁵N Spin Relaxation Parameters

Peak volumes for $^{1}\text{H}^{\text{N}}_{-}^{1}5\text{N}$ correlation peaks were integrated using the program XEASY(22). T_{1} , $T_{1\text{p-CPMG}}$, and $T_{1\text{p-CW}}$ relaxation times were extracted by fitting of a single exponential function to these volumes by use of the CURVE_FIT program which is part of the MODELFREE package(34,35). Out of 165 possible peaks (arising from 184 residues

minus 10 residues of the *Strep-tag* II, 8 prolyl residues and the N-terminal residue), 140 and 145 were considered for, respectively, FluA(R95K) and the FluA(R95K)•fluorescein complex. Other peaks were overlapped to an extent that prevented accurate integration, or were broadened beyond detection and remained unassigned [FluA(R95K): backbone amide moieties of residues 61, 112, 113, 128; FluA(R95K)•fluorescein: 26, 69, 118, 128].

For both FluA(R95K) and the FluA(R95K)•fluorescein complex, axially symmetric diffusion tensors were calculated based on (i) three-dimensional structure and hydrodynamic theory using the program HYDRONMR(36) and (ii) ^{15}N spin relaxation parameters using the programs MODELFREE(34,35) and FAST-MODELFREE(37). Both approaches consistently revealed that the overall rotational tumbling time can be very well described with a single correlation time, τ_c , characterizing isotropic reorientation (the ratios of parallel over orthogonal components, D_\parallel/D_\perp , for the axially symmetric diffusion tensors turned out to be $\sim\!1.1$). Hence, model-free calculations to fit ^{15}N spin relaxation parameters were performed assuming isotropic rotational diffusion. Moreover, to ensure conservative data interpretation, a simple approach was chosen considering solely a squared order parameter, S^2 , and the overall rotational correlation time, τ_c

Residues involved in slow internal motional modes were identified by comparing $T_{1\rho\text{-CW}}$ and $T_{1\rho\text{-CPMG}}$ relaxation times, using the criteria that $T_{1\rho\text{-CW}} - T_{1\rho\text{-CPMG}} > 10$ ms while the corresponding 2σ intervals do not overlap.

Isothermal Titration Calorimetry

Isothermal titration calorimetry was performed at 25 °C in a MicroCal (Central Milton Keynes, UK) VP-ITC instrument. 1.431 mL of a 4 μM solution of FluA(R95K) in phosphate buffered saline (PBS: 4 mM KH₂PO₄, 16 mM Na₂HPO₄, 115 mM NaCl, pH 7.4) was titrated with 4 μl aliquots of a 100 μM solution of fluorescein (disodium salt) in the same buffer. Data analysis was performed using version 7.0 of the instrument software assuming the standard model of bimolecular complex formation.

Results and Discussion

Completion of Resonance Assignment for FluA(R95K)

Nearly complete resonance assignments were obtained for FluA(R95K) as described by Liu et al(15). Using biosynthetically directed, fractional $^{13}\text{C-labeled}(17,18)$ FluA(R95K), those data were complemented by the stereo-specific assignment of the methyl groups for 8 out of 13 Val residues with non-degenerate $^1H^{\gamma/13}C^{\gamma}$ chemical shifts (62%) and for all 5 Leu residues of FluA(R95K). The GLOMSA(38) and FOUND(38) subroutines of DYANA(23) provided additional stereospecific assignments for 4 out of 15 (27%) Gly α -methylene protons with non-degenerate $^1H^{\alpha}$ chemical shifts, for 19 out of 99 β -methylene protons with non-degenerate $^1H^{\beta}$ chemical shifts (19%), for 2 more peripheral methylene protons (Pro 9 $^1H^{\gamma}$ and Pro 13 $^1H^{\delta}$), and for the methyl groups of 2 further Val residues with non-degenerate $^1H^{\gamma/13}C^{\gamma}$ chemical shifts.

NMR Structure of FluA(R95K)

The NMR structure (Table 1, Figure 2) of FluA(R95K) was calculated based on 2089 conformationally-restricting $^1H^{-1}H$ distance constraints and 258 backbone dihedral constraints. The statistics of the NMR structure of FluA(R95K) show that a high-quality structure was obtained (Table 1), which is visually apparent (Figure 2). A technical comment relates to the fact that FluA(R95K) and the C-terminal *Strep-tag* II contain a high fraction (18%) of aromatic residues (5 Phe, 7 His, 7 Trp, and 15 Tyr). The resulting spectral overlap impedes resonance assignment and identification of upper distance limit constraints

when using data recorded at ¹H resonance frequencies of 600 and 750 MHz. However, 2D [¹H, ¹H]-NOESY acquired at 900 MHz yielded almost complete resonance assignments for all 34 aromatic residues(15), resulting in 367 additional distance constraints. Comparative structure calculations demonstrated the impact on the precision of the final NMR solution structure (Table 1).

FluA(R95K) exhibits the characteristic lipocalin fold defined by eight antiparallel β -strands forming an almost circular β -barrel(2). In addition to the conserved β -strands (A through H), two smaller β -strands (A' and H') were identified outside the barrel region, as well as three α -helices (I to III). The β -strands (A', A to H, and H', respectively) include residues 2-4, 24-31, 42-49, 54-62, 65-75, 83-90, 93-104, 109-118, 123-132, and 161-162 (Figure 2). The three α -helices (I through III) comprise residues 139-151, 157-159, and 167-170. Of these, helix I corresponds to the α -helix that is structurally conserved throughout the lipocalin family and is typically seen attached to one side of the β -barrel(2). Calculation of local backbone r.m.s.d. values and global backbone displacements (Figure 2C) revealed that all β -strands are locally and globally well defined, whereas several of the loops connecting the regular secondary structure elements at the open end of the barrel are both locally and globally rather ill-defined.

A short polypeptide segment close to the N-terminus comprising residues 19-21 contributes to closing one end of the β -barrel (the "bottom" in Figure 2). In contrast, the other end of the β -barrel (the "top" in Figure 2) is open to solvent and flanked by four large loops, which clearly appear to be more flexibly disordered in the ensemble of NMR conformers. β -strands E and F extend away from the β -barrel near the open end and form a hairpin loop. Notably, the conserved α -helix I forms contacts with β -strands F, G, and H, thereby burying several hydrophobic side chains, which gives rise to a second hydrophobic core region on the outside of the β -barrel supersecondary structure(2).

Comparison with the Crystal Structures of the FluA•fluorescein and BBP•biliverdin complexes

The NMR structure of FluA(R95K) shows a remarkable global similarity when compared with either the crystal structure of the FluA•fluorescein complex(10) or the crystal structure of the BBP•biliverdin complex(5), *i.e.* the natural lipocalin on which the combinatorial design of FluA was based(6) (Figures 1-3). Superposition of the 58 C^{α} -atoms of the β -barrel [the conserved structural feature across the lipocalin family(2)] yielded r.m.s.d. values of 1.57 Å [FluA(R95K) and FluA•fluorescein] and 1.70 Å [FluA(R95K) and BBP•biliverdin].

However, larger r.m.s.d. values of 2.29 Å and of 2.62 Å were obtained when all 173 C^{α} positions of the crystallographically defined residues were used for the superposition. Considering that apart from the conserved β -barrel motif also the α -helices are almost identical in these structures, these values indicate that the loop regions at both ends of the β -barrel show larger structural variability than the regular secondary structure elements themselves. Among the four loops at the open end of the β -barrel, which form the entrance to the ligand pocket, loop 1 (connecting strands A and B) shows the largest conformational variability.

In the BBP•biliverdin complex, this loop assumes a rather compact conformation, including a short 3_{10} -helix, whereas in FluA•fluorescein this loop adopts a more extended conformation. The NMR structure of the uncomplexed FluA(R95K) reveals a similar conformation, but the tip of this loop slightly swings out from the central axis of the β -barrel. Moreover, the 3_{10} -helix observed in the X-ray structures of the complexes was not apparent in the NMR structure of the apo-protein. However, the chemical shifts of the polypeptide backbone of residues 19-21 are in the range expected for a helical conformation.

It might thus well be that the 3_{10} -helix is formed only transiently in the apo-protein, and further stabilized upon complex formation.

The extended conformation of loop 1 in the engineered lipocalin FluA(R95K) apparently arises from the four side chain substitutions at its tip (from Asn-Ser-Val-Glu 34-38 in BBP to Ser-Pro-Asn-Gly). Regarding the other three loops at the open end of the β -barrel, loop 4 (connecting strands G and H) is most similar in all three structures. For loop 3 (connecting strands E and F), which shows a large movement at its tip when comparing FluA•fluorescein with BBP•biliverdin, an intermediate position is observed in the NMR structure of the uncomplexed FluA(R95K). Contrastingly, for loop 2 (connecting strands C and D), which is bent more toward the central axis in FluA•fluorescein when compared with BBP•biliverdin, its tip is even closer to the axis in FluA(R95K).

When looking into the deep cavity for the fluorescein ligand, it appears that this pocket is already pre-shaped in FluA(R95K). In particular, the side chain of Trp 129, which closely packs against the xanthelonone moiety of fluorescein in the crystal structure and has been considered essential for the observed fluorescence quenching effect(8), assumes a very similar rotameric state. In fact, the indole side chain of Trp 129 is coplanar with the ligand in the FluA•fluorescein complex while the conformation of this non-mutated residue is quite different in BBP•biliverdin(5,10), with large dihedral angle changes of $\Delta_{\chi}^{1} = 130^{\circ}$ and $\Delta_{\chi}^{2} =$ 175°. In contrast, the conformation of Trp 129 in FluA(R95K) is almost the same as in FluA•fluorescein, demonstrating that its altered geometry is primarily caused by the introduction of the surrounding mutations rather than comprising an induced fit upon ligand binding (Figure 3). Nevertheless, small dihedral angle changes are observed when comparing FluA(R95K) with FluA•fluorescein, which are structurally relevant as the indole moiety of Trp 129 in the free protein occupies a portion of the cavity which is filled in the complex by the incoming fluorescein ligand. In fact, mutation of Trp 129 to any other aromatic residue (Phe, Tyr, or His; with the largest adverse effect for His) significantly weakens the interaction between FluA and fluorescein (K_D increased from 35 nM to 8.6 μ M) and also reduces the fluorescence quenching effect from nearly 100% to 30% (39).

Phe 99, on the other hand, exhibits a χ^1 -rotameric state in the NMR structure that differs by $\Delta_{\chi}^1 = 65^{\circ}$ from the crystallized FluA•fluorescein complex, while its conformation in the free FluA(R95K) is very similar to the one in the BBP•biliverdin complex. Hence, Phe 99, which was not exchanged during engineering of FluA, together with the side chain of the residue Arg 88 in its vicinity, which had been mutated during generation of FluA from BBP (Figure 3), reveal a pronounced "induced fit" upon complex formation. Consistently, this region was previously identified as crucial for the engineered ligand binding activity(10).

Backbone Dynamics of FluA(R95K) and FluA(R95K)•Fluorescein

The assignment of backbone ^{15}N and $^{1}H^{N}$ chemical shifts is necessary for residue specific assessment of biomolecular dynamics. For the FluA(R95K)•fluorescein complex, which was prepared by titrating the free protein solution with fluorescein, nearly complete assignment (97%) of the ^{15}N , ^{13}C , and $^{1}H^{N}$ backbone and $^{13}C^{\beta}$ resonances was obtained, excluding only (i) $^{13}C'$ shifts of residues preceding prolyl residues or preceding residues Lys 25, Trp 26, Phe 68, Tyr 117, His 127, (ii) the amide resonances of Trp 26, Met 69, Asp 118, Val 128, (iii) the $^{13}C^{\alpha}$ resonances of Trp 26, and (iv) the $^{13}C^{\beta}$ resonances of Trp 26, Trp 27, Pro 35, Cys 42, Arg 58, Tyr 59, Asp 60, His 63, Met 69, Lys 121, and Lys 122. Chemical shift perturbations (Figure 1) were observed only for the β -barrel, and inspection of the FluA•fluorescein structure revealed that the largest shift perturbations can be attributed to ring current effects from the extended aromatic system of the bound ligand.

Fitting of relaxation parameters (see Supplemental Material) yielded about the same correlation time (~13 ns) for the overall rotational tumbling of FluA(R95K) and of FluA(R95K)•fluorescein. Moreover, pronounced changes of order parameters were not registered upon complex formation (see Supplemental Material). In contrast, a remarkable reduction and redistribution of slow motional modes was observed by comparing T_{1p-CW} and $T_{Ip\text{-CPMG}}$ relaxation times or identification of excessive exchange broadening of peaks in the 2D [15N, 1H]-HSQC spectra (Figure 4). While in FluA(R95K) at least 26 residues (7, 19, 23, 39, 44, 56, 59, 60, 64, 69, 72, 85, 86, 89, 90, 94-98, 108, 115, 121, 126, 154, and 166) are involved in slower motional modes, only 10 such residues (2, 19, 44, 93, 98, 119, 152, 155, 156, and 166) were identified in the FluA(R95K)•fluorescein complex. Only four residues are common to both subsets (19, 44, 98, and 166): Trp 19 and Ser 166 are located in more remote segments while Trp 44 and Val 98 are located in spatial proximity to the fluorescein binding site. The remaining 6 residues [with respect to FluA(R95K)•fluorescein] are either not in spatial proximity to the ligand pocket (2, 119, 152, 155, and 166) or not observed in the spectra of FluA(R95K) (93). In FluA(R95K), most of the residues affected by slower motional modes are located within the β-barrel, in particular residues 85, 86, and 94-98, which also exhibit the largest chemical shift perturbation upon complex formation. For FluA(R95K), residues with such identified slow conformational exchange are located in polypeptide segments exhibiting well increased local r.m.s.d. values in the NMR structure, indicating that the lower precision arises from increased flexibility (in particular for segments in the loop regions at the open end of the β-barrel; Figures 2 and 4; note that increased r.m.s.d. values in other polypeptide segments are due to either fast internal motions on the ns times-scale and/or lack of conformational constraints). Taken together, the comparison of slow motional modes clearly indicates that the β -barrel is rigidified upon complex formation. This may well be the reason why the FluA•fluorescein complex readily crystallized, while diffraction quality crystals of the apo-protein have thus far not been obtained.

Isothermal Titration Calorimetry

An investigation of the thermodynamics of fluorescein binding using isothermal titration calorimetry (ITC) revealed that ligand binding is entirely enthalpy driven (Figure 5). This is consistent with the rigidification of the protein upon complex formation as observed in the NMR study. Evaluation of the calorimetry data using the standard model of bimolecular complex formation resulted in a stoichiometry of 1.06 binding sites per protein molecule and an affinity constant of $2.20 \pm 0.12 \cdot 10^7$ M⁻¹. The deduced K_D value of 45 nM is very close to the value of 35 nM earlier determined via fluorescence titration(6). Ligand binding was accompanied by a high exothermic change in enthalpy (-16.5 kcal mol⁻¹) and by a strongly negative change in entropy (-21.6 cal K⁻¹ mol⁻¹).

Conclusions

We have solved the three-dimensional solution structure of the anticalin FluA(R95K), which has engineered binding specificity for the prescribed ligand fluorescein. A comparison with the crystal structures of the FluA•fluorescein complex and the native BBP•biliverdin complex revealed the role of several side chains in the ligand pocket for the recognition of the new ligand. Furthermore, the solution structure of FluA(R95K) allowed identification of important structural rearrangements that are either due to the amino acid exchanges in the binding site, to complex formation with the ligand, or to a combination of both. In particular, we were able to identify an induced fit mechanism resulting in a concerted side chain rearrangement of several residues at the bottom of the ligand pocket. It is tempting to speculate that the slow motional modes detected for β -strands E and F might possibly related to a transient opening of the upper part of the β -barrel, which allows the ligand to access the

binding pocket. Thus, our investigation provides insight into both the static features of the ligand-binding site of an engineered lipocalin in solution and into its dynamic properties. These findings from high resolution NMR analysis illustrate the remarkable ability of the lipocalin fold to provide cognate binding pockets for many different ligands. In fact, a role of internal dynamics for ligand recognition has not become apparent for several natural and engineered lipocalins which were previously characterized by X-ray crystallography – for example retinol-binding protein / retinol(40), apolipoprotein D / progesterone(41), DigA16 / digoxigenin(11) – revealing just minute structural changes between the apo- and holo-states. In one recently published example of an engineered lipocalin that recognizes the extramembrane domain of the T-cell coreceptor CTLA-4 an enhanced flexibility of the loop region in the apo-protein as well as induced fit and rigidification upon binding of the target was observed by X-ray analysis, while changes in the structure of the β-barrel were not detectable (42). Notably, in the case of the major urinary protein (MUP), a natural lipocalin from mouse, the opposite behavior was observed: NMR relaxation experiments indicated that the backbone flexibility in fact increases upon binding of the mouse pheromone 2-secbutyl-4,5-dihydrothiazole(43). However, this phenomenon seems not to be fully understood yet(44,45). Taken together, these new insights into structure and dynamics as well as thermodynamics of lipocalin-ligand interactions do not only shed new light on the mechanisms of ligand recognition but will also support future design of anticalins with novel specificities.

Supplementary Material

Refer to Web version on PubMed Central for supplementary material.

Acknowledgments

A.S. thanks S. Danzer and I. Theobald for expert technical assistance, and T.S. thanks the UB Center of Computational Research (CCR) for support.

This work was supported by the Protein Structure Initiative of the National Institutes of Health (U54-GM074958) and the National Science Foundation (MCB 0416899 and 0817857 to T.S.).

Abbreviations

BBP bilin-binding protein

FluA engineered lipocalin with specificity for fluorescein

NMR nuclear magnetic resonance NOE nuclear Overhauser effect

References

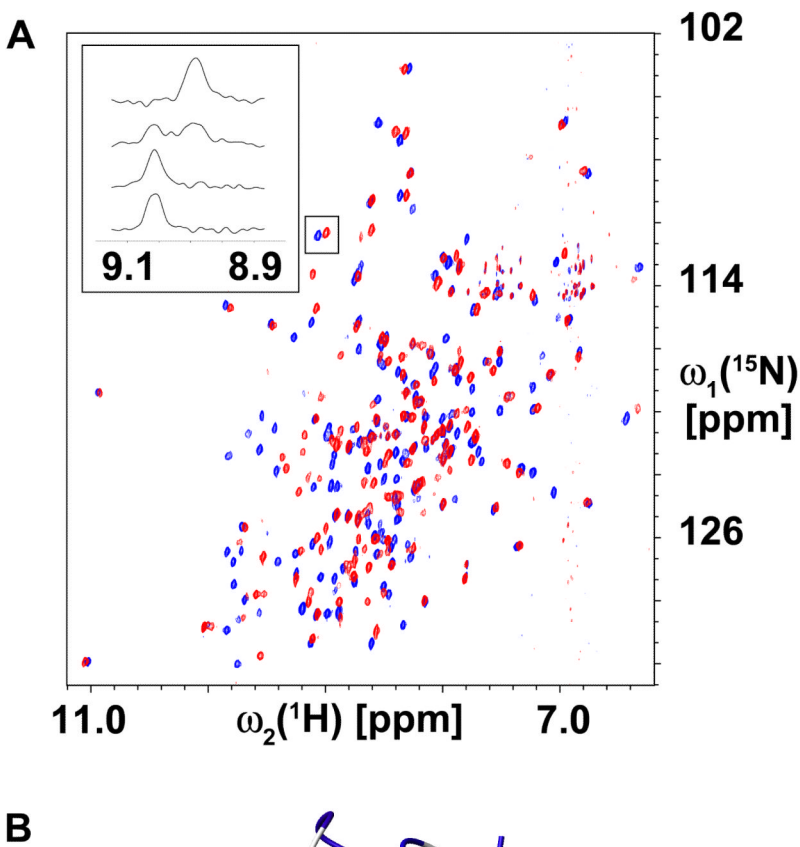
- 1. Flower DR. The lipocalin protein family: structure and function. Biochem J 1996;318:1–14. [PubMed: 8761444]
- Skerra A. Lipocalins as a scaffold. Biochim Biophys Acta 2000;1482:337–350. [PubMed: 11058774]
- 3. Skerra A. Imitating the humoral immune response. Curr Opin Chem Biol 2003;7:683–693. [PubMed: 14644176]
- Skerra A. Alternative binding proteins: anticalins harnessing the structural plasticity of the lipocalin ligand pocket to engineer novel binding activities. FEBS Lett 2008;275:2677–2683.
- 5. Huber R, Schneider M, Mayr I, Müller R, Deutzmann R, Suter F, Zuber H, Falk H, Kayser H. Molecular structure of the bilin binding protein (BBP) from *Pieris brassicae* after refinement at 2.0 Å resolution. J Mol Biol 1987;198:499–513. [PubMed: 3430616]

 Beste G, Schmidt FS, Stibora T, Skerra A. Small antibody-like proteins with prescribed ligand specificities derived from the lipocalin fold. Proc Nat Acad Sci U S A 1999;96:1898–1903.

- 7. Voss, EW, Jr. Fluorescein Hapten: An Immunological Probe. CRC Press; Boca Raton, FL: 1984.
- 8. Götz M, Hess S, Beste G, Skerra A, Michel-Beyerle ME. Ultrafast electron transfer in the complex between fluorescein and a cognate engineered lipocalin protein, a so-called anticalin. Biochemistry 2002;41:4156–4164. [PubMed: 11900559]
- 9. Schlehuber S, Beste G, Skerra A. A novel type of receptor protein, based on the lipocalin scaffold, with specificity for digoxigenin. J Mol Biol 2000;297:1105–1120. [PubMed: 10764576]
- 10. Korndörfer IP, Beste G, Skerra A. Crystallographic analysis of an "anticalin" with tailored specificity for fluorescein reveals high structural plasticity of the lipocalin loop region. Proteins: Struct Funct Genet 2003;53:121–129. [PubMed: 12945055]
- 11. Korndörfer IP, Schlehuber S, Skerra A. Structural mechanism of specific ligand recognition by a lipocalin tailored for the complexation of digoxigenin. J Mol Biol 2003;330:385–396. [PubMed: 12823976]
- Breustedt DA, Korndörfer IP, Redl B, Skerra A. The 1.8-Å crystal structure of human tear lipocalin reveals an extended branched cavity with capacity for multiple ligands. J Biol Chem 2005;280:484–493. [PubMed: 15489503]
- 13. Jameson GB, Adams JJ, Creamer LK. Flexibility, functionality and hydrophobicity of bovine ®-lactoglobulin. Int Dairy J 2002;12:319–329.
- 14. Cowan SW, Newcomer ME, Jones TA. Crystallographic refinement of human serum retinol binding protein at 2A resolution. Proteins: Struct Funct Genet 1990;8:44–61. [PubMed: 2217163]
- Liu G, Mills JL, Hess TA, Kim S, Skalicky JJ, Sukumaran DK, Kupce E, Skerra A, Szyperski T. Resonance assignments for the 21 kDa engineered fluorescein-binding lipocalin FluA. J Biomol NMR 2003;27:187–188. [PubMed: 12913418]
- 16. Schmidt TG, Skerra A. The *Strep*-tag system for one-step purification and high-affinity detection or capturing of proteins. Nat Protoc 2007;2:1528–1535. [PubMed: 17571060]
- 17. Neri D, Szyperski T, Otting G, Senn H, Wüthrich K. Stereospecific nuclear magnetic resonance assignments of the methyl groups of valine and leucine in the DNA-binding domain of the 434 repressor by biosynthetically directed fractional ¹³C labeling. Biochemistry 1989;28:7510–7516. [PubMed: 2692701]
- Szyperski T, Neri D, Leiting B, Otting G, Wuthrich K. Support of 1H NMR assignments in proteins by biosynthetically directed fractional 13C-labeling. J Biomol NMR 1992;2:323–334. [PubMed: 1324756]
- 19. Cavanagh, J.; Fairbrother, WJ.; Palmer, AGI.; Rance, M.; Skelton, NJ. Protein NMR spectroscopy: Principles and practice. Second. Elsevier Academic Press; San Diego: 2007.
- 20. Vuister GW, Bax A. Quantitative J correlation: a new approach for measuring homonuclear three-bond $J_{\rm HN}{\rm H}\alpha$ coupling constants in 15N-enriched proteins. J Am Chem Soc 1993;115:7772–7777.
- 21. Güntert P, Dötsch V, Wider G, Wüthrich K. Processing of multi-dimensional NMR data with the new software PROSA. J Biomol NMR 1992;2:619–629.
- 22. Bartels C, Xia Th, Billeter M, Güntert P, Wüthrich K. The program XEASY for computer-supported NMR spectral analysis of biological macromolecules. J Biomol NMR 1995;6:1–10.
- 23. Güntert P, Mumenthaler C, Wüthrich K. Torsion angle dynamics for NMR structure calculation with the new program DYANA. J Mol Biol 1997;273:283–298. [PubMed: 9367762]
- 24. Cornilescu G, Delaglio F, Bax A. Protein backbone angle restraints from searching a database for chemical shift and sequence homology. J Biomol NMR 1999;13:289–302. [PubMed: 10212987]
- 25. Koradi R, Billeter M, Wüthrich K. MOLMOL: a program for display and analysis of macromolecular structures. J Mol Graph 1996;14:51–55. 29–32. [PubMed: 8744573]
- Grzesiek S, Bax A. Improved 3D triple-resonance NMR techniques applied to a 31 kDa protein. J Magn Res 1992;96:432–440.
- 27. Wittekind M, Mueller L. HNCACB, a High-Sensitivity 3D NMR Experiment to Correlate Amide-Proton and Nitrogen Resonances with the Alpha- and Beta-Carbon Resonances in Proteins. J Magn Res Ser B 1993;101:201–205.

28. Yamazaki T, Lee W, Arrowsmith CH, Muhandiram DR, Kay LE. A Suite of Triple Resonance NMR Experiments for the Backbone Assignment of 15N, 13C, 2H Labeled Proteins with High Sensitivity. J Am Chem Soc 1994;116:11655–11666.

- 29. Farrow NA, Muhandiram R, Singer AU, Pascal SM, Kay CM, Gish G, Shoelson SE, Pawson T, Forman-Kay JD, Kay LE. Backbone dynamics of a free and a phosphopeptide-complexed Src homology 2 domain studied by ¹⁵N NMR relaxation. Biochemistry 1994;33:5984–6003. [PubMed: 7514039]
- Orekhov VY, Pervushin KV, Arseniev AS. Backbone dynamics of (1-71)bacterioopsin studied by two-dimensional ¹H-¹⁵N NMR spectroscopy. Eur J Biochem 1994;219:887–896. [PubMed: 8112340]
- 31. Szyperski T, Luginbühl P, Otting G, Güntert P, Wüthrich K. Protein dynamics studied by rotating frame ¹⁵N spin relaxation times. J Biomol NMR 1993;3:151–164. [PubMed: 7682879]
- 32. Kay LE, Nicholson LK, Delaglio F, Bax A, Torchia DA. Pulse sequences for removal of the effects of cross correlation between dipolar and chemical-shift anisotropy relaxation mechanisms on the measurement of heteronuclear T1 and T2 values in proteins. J Magn Res 1992;97:359–375.
- 33. Palmer AGI, Skelton NJ, Chazin WJ, Wright PE, Rance M. Suppression of the effects of cross correlation between dipolar and anisotropic chemical-shift relaxation mechanisms in the measurement of spin-spin relaxation rates. Mol Phys 1992;75:699–711.
- 34. Palmer AG III, Rance M, Wright PE. Intramolecular motions of a zinc finger DNA-binding domain from Xfin characterized by proton-detected natural abundance carbon-13 heteronuclear NMR spectroscopy. J Am Chem Soc 1991;113:4371–4380.
- 35. Mandel AM, Akke M, Palmer AG III. Backbone dynamics of Escherichia coli ribonuclease HI: correlations with structure and function in an active enzyme. J Mol Biol 1995;246:144–163. [PubMed: 7531772]
- Garcia de la Torre J, Huertas ML, Carrasco B. HYDRONMR: prediction of NMR relaxation of globular proteins from atomic-level structures and hydrodynamic calculations. J Magn Res 2000;147:138–146.
- 37. Cole R, Loria JP. FAST-Modelfree: A program for rapid automated analysis of solution NMR spin-relaxation data. J Biomol NMR 2003;26:203–213. [PubMed: 12766418]
- 38. Güntert P, Braun W, Wüthrich K. Efficient computation of three-dimensional protein structures in solution from nuclear magnetic resonance data using the program DIANA and the supporting programs CALIBA, HABAS and GLOMSA. J Mol Biol 1991;217:517–530. [PubMed: 1847217]
- 39. Vopel S, Muhlbach H, Skerra A. Rational engineering of a fluorescein-binding anticalin for improved ligand affinity. Biol Chem 2005;386:1097–1104. [PubMed: 16307475]
- 40. Zanotti G, Ottonello S, Berni R, Monaco HL. Crystal structure of the trigonal form of human plasma retinol-binding protein at 2.5 A resolution. J Mol Biol 1993;230:613–624. [PubMed: 8464067]
- 41. Eichinger A, Nasreen A, Kim HJ, Skerra A. Structural insight into the dual ligand specificity and mode of high density lipoprotein association of apolipoprotein D. J Biol Chem 2007;282:31068–31075. [PubMed: 17699160]
- 42. Schönfeld D, Matschiner G, Chatwell L, Trentmann S, Gille H, Hulsmeyer M, Brown N, Kaye PM, Schlehuber S, Hohlbaum AM, Skerra A. An engineered lipocalin specific for CTLA-4 reveals a combining site with structural and conformational features similar to antibodies. Proc Natl Acad Sci U S A 2009;106:8198–8203. [PubMed: 19416843]
- 43. Zidek L, Novotny MV, Stone MJ. Increased protein backbone conformational entropy upon hydrophobic ligand binding. Nat Struct Biol 1999;6:1118–1121. [PubMed: 10581552]
- 44. Kuser PR, Franzoni L, Ferrari E, Spisni A, Polikarpov I. The X-ray structure of a recombinant major urinary protein at 1.75 Å resolution. A comparative study of X-ray and NMR-derived structures. Acta Crystallogr D Biol Crystallogr 2001;57:1863–1869. [PubMed: 11717500]
- 45. Perazzolo C, Wist J, Loth K, Poggi L, Homans S, Bodenhausen G. Effects of protein-pheromone complexation on correlated chemical shift modulations. J Biomol NMR 2005;33:233–242. [PubMed: 16341752]



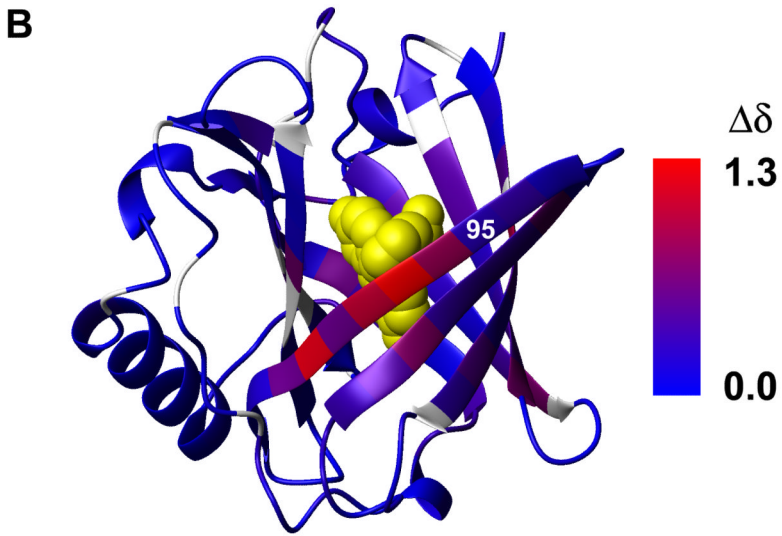


Figure 1. (A) 2D [15 N, 1 H]-HSQC spectra recorded for FluA(R95K) (red contour plot) and for FluA(R95K)•fluorescein (blue contour plot). The insert shows cross sections taken along $\omega_2(^{1}H^N)$ at the $\omega_1(^{15}N)$ shift of residue Gly 40 (boxed peaks beside the insert) from spectra acquired during the progress of the titration of FluA(R95K) with fluorescein (from bottom to top: 0%, 25%, 50%, and 100% completion). (B) The chemical shift differences observed between FluA(R95K) and FluA(R95K)•fluorescein [calculated as $\Delta\delta=(0.1\times\Delta\delta_N^2+\Delta^2)^{1/2}$] are mapped onto a ribbon drawing of the X-ray structure of the FluA•fluorescein complex(10). Color scheme: segments in grey indicate missing resonance assignments or Pro residues, for segments in blue $^{1}H^N$ and ^{15}N shifts remain (virtually) unchanged upon

complex formation, while for segments in red the largest changes are observed [individual chemical shift changes of up to $0.8(^1H^N)$ and $3.7(^{15}N)$ ppm for residues Thr 97 and Asn 100, respectively, and a maximum $\Delta\delta$ of 1.3 for Thr 97]. The C^α position of the R95K mutation, which is not involved in ligand contacts and does not affect fluorescein binding, is labeled.

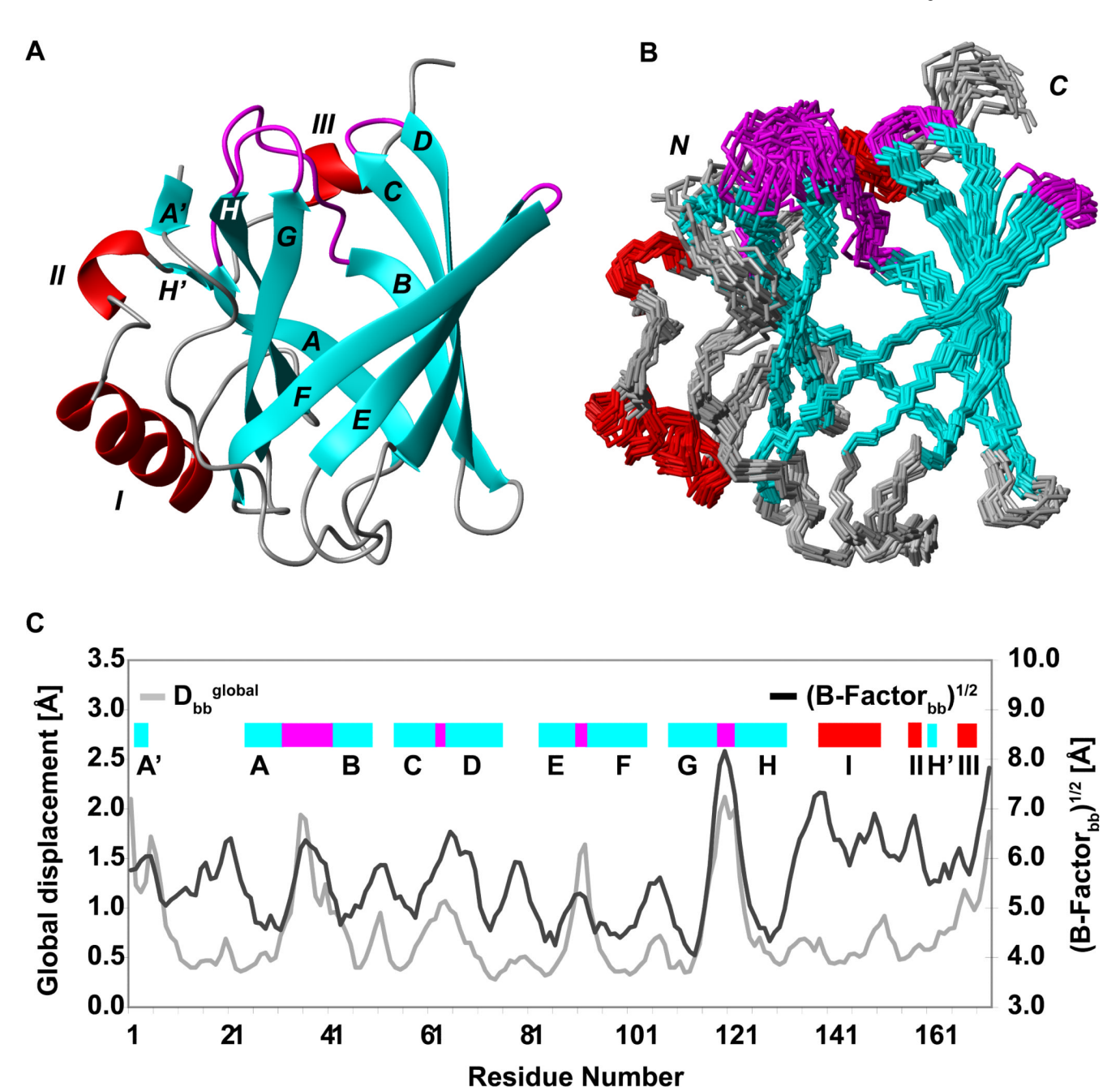


Figure 2. NMR structure of uncomplexed FluA(R95K). (A) Ribbon drawing of the NMR structure derived from the DYANA conformer with the lowest target function value. The β -strands (A ', A - H, H') and the α-helices (I - III) are depicted in cyan and red, respectively, while the four flexible loops that form the entrance to the binding site are shown in magenta. Other regions are depicted in gray. (B) The ensemble of 20 DYANA conformers selected to represent the NMR solution structure is shown after superposition of the backbone heavy atoms (N, Cα, and C') in regular secondary structure elements (Table 1) and colored as in (A). (C) The global backbone displacements (D_{bb}global; left vertical axis) of the NMR structure of FluA(R95K) are plotted versus amino acid sequence and represented by a grey line. For comparison, the average square root of the B-factors of backbone heavy atoms of

each residue (B-Factor_{bb} $^{1/2}$, right vertical axis) in the X-ray structure of the FluA•fluorescein complex (PDB code 1N0S, chain A) is also plotted versus the sequence and represented by a black line. The location of α -helices and β -strands are indicated, respectively, with red and cyan bars, while the mutagenized loop segments at the "open" end of the β -barrel are represented as magenta bars.

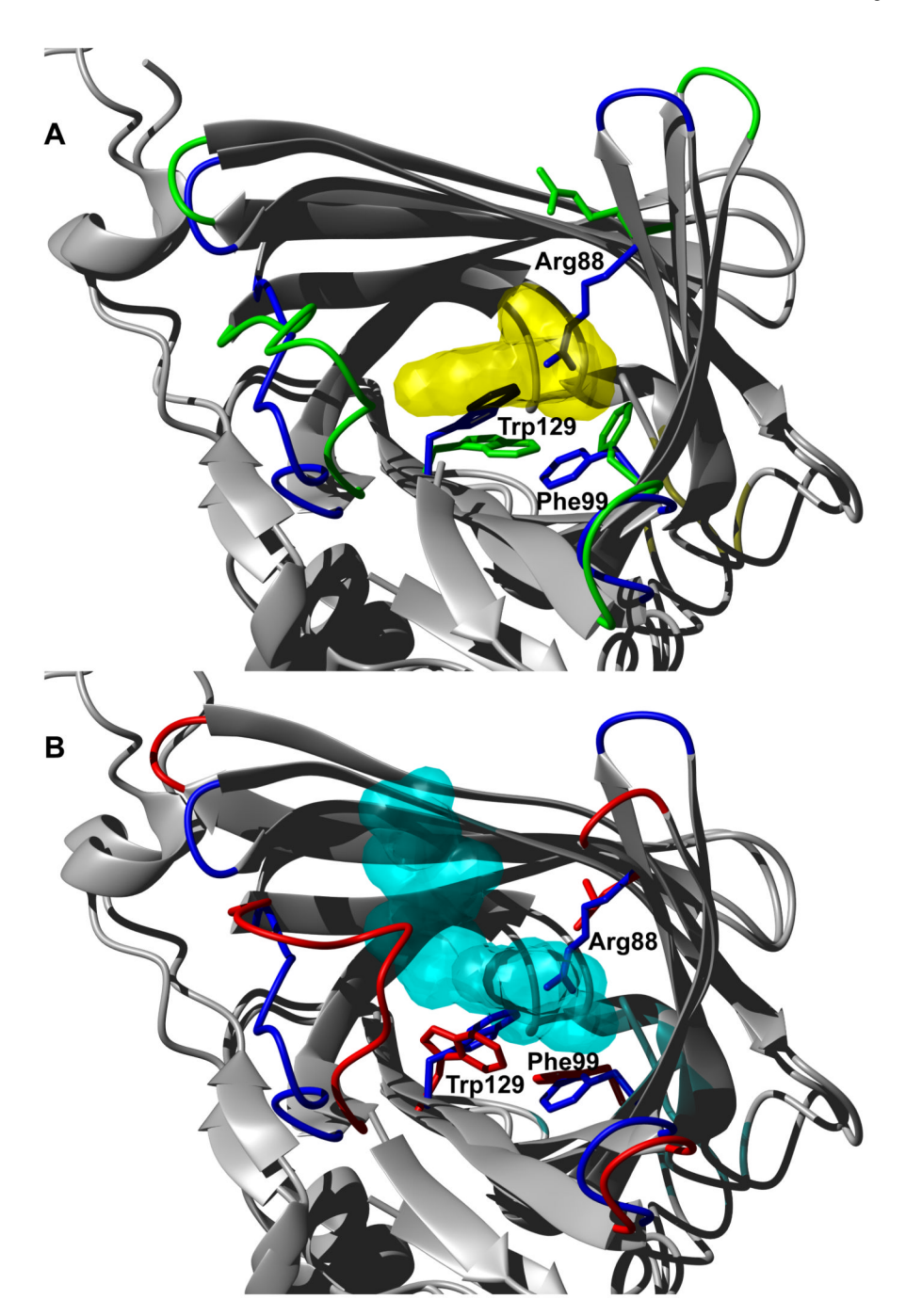


Figure 3. Structural superposition of the NMR structure of FluA(R95K) (this study; 1T0V, model 1; blue) with (A) the crystal structure of the FluA•fluorescein complex (1N0S; chain A; green) or (B) the crystal structure of BBP•biliverdin (1BBP; chain A; red) using the heavy backbone atoms of the regular secondary structure elements (Table 1). The molecular surfaces of the ligands fluorescein (1N0S; yellow) and biliverdin IX_{γ} (1BBP; cyan) are shown. The side chains of Arg 88, Phe 99, and Trp 129 (Leu, Phe, and Trp, respectively, in the case of BBP) are depicted as sticks for all three models and illustrate rearrangements upon fluorescein binding to FluA (in particular, Arg 88 and Phe 99).

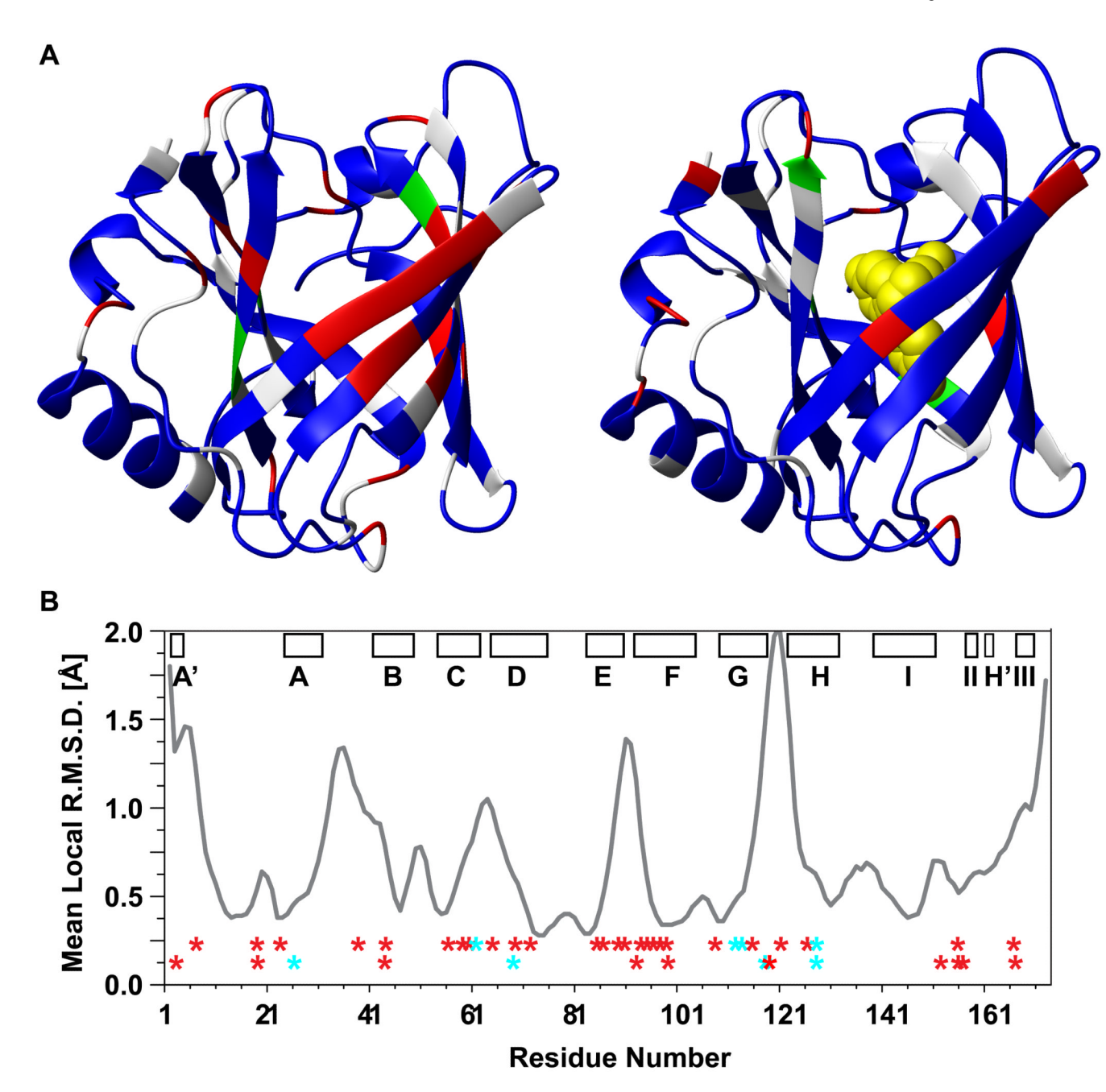


Figure 4. (A) Ribbon diagrams of the NMR structure of FluA(R95K) to represent presence and absence of slower motional modes colored in red and blue, respectively, detected by measurement of rotating frame transverse 15 N spin relaxations times [on the left: FluA(R95K), on the right: the NMR structure FluA(R95K) with the bound fluorescein ligand from the crystal structure (1N0S) displayed in yellow]. In both cases, green is used to highlight residues that remained unassigned and white indicates Pro or overlapping peaks that were not integrated. (B) Mean local r.m.s.d. values were calculated for backbone heavy atoms N, C^{α} and C' of tripeptide segments and assigned to the middle residue of the segment. Those are plotted versus the amino acid sequence. The bars represent helices, strands, and loops as in Figure 2. For comparison, the top and bottom rows of red and cyan

asterisks (*) indicate, respectively, residues in FluA(R95K) or in the FluA(R95K)•fluorescein complex for which slow conformational exchange was inferred from comparison of $T_{1\rho}$ -relaxation times (red) and detection of excessive exchange broadening in the HSQC-spectra (green).

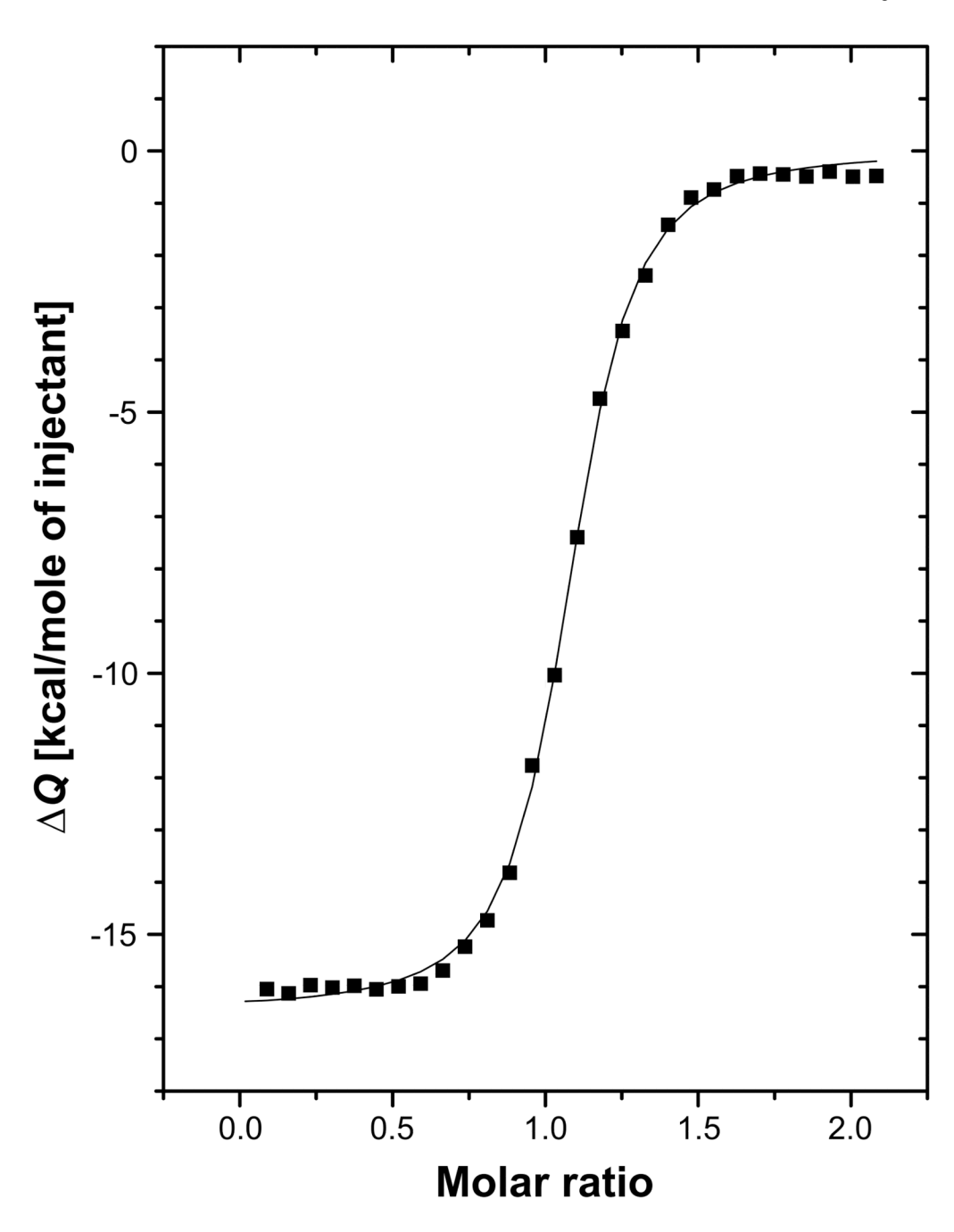


Figure 5. Isothermal titration calorimetry (ITC) of FluA(R95K) with fluorescein in PBS at 25 °C in a MicroCal instrument. Data analysis according to the standard model of 1:1 complex formation resulted in N = 1.06 binding sites with $K_A = 2.20 \pm 0.12 \cdot 10^7 \ M^{-1}$, $\Delta H = -16,460 \pm 73$ cal mol⁻¹ and $\Delta S = -21.6$ cal K^{-1} mol⁻¹.

Table 1 Statistics of FluA(R95K) NMR structure determination.

Completeness of resonance assignments [%]	
backbone a	97%
side chains b	95%
stereospecific assignments $^{\mathcal{C}}$	
^a CH ₂ of glycines	27%
$^{ m eta}{ m CH}_2$	20%
Val and Leu isopropyl groups	79%
Conformationally restricting distance constraints	
intra-residue	540 (549)
sequential	597 (566)
medium range	267 (181)
long range	685 (426)
total	2089 (1722)
Didedral angle constraints	
φ	154
Ψ	104
Number of constraints per residue	12.8
Number of long range constraints per residue	3.7
DYANA target function [Å ²]	$1.81 \pm 0.13 \; (1.54 \pm 0.26)$
Average r. m. s. d. to the mean DYANA coordinates $[\mathring{A}]$ regular secondary structure elements	$0.71 \pm 0.11 \; (1.00 \pm 0.19)$
backbone heavy atoms (N, C^{α}, C')	
regular secondary structure, all heavy atoms	$1.14 \pm 0.15 \; (1.57 \pm 0.17)$
residues 2-170, backbone heavy atoms N, C^{α} , C'	$0.81 \pm 0.12 \; (1.23 \pm 0.21)$
residues 2-170, all heavy atoms	$1.22 \pm 0.13 \; (1.76 \pm 0.18)$
heavy atoms of molecular $core^d$	1.14 ± 0.15
Ramachandran plot summary for residues 2-170 (regular secondary elements) [%]	
most favorable regions	71 (82)
additionally allowed regions	24 (17)
generously allowed regions	3 (1)
disallowed regions	2 (0)
Average number of distance constraint violation	
per DYANA conformer [Å]	
0.2 - 0.5	2
>0.5	0
Average number of dihedral angle constraint violations per DYANA conformer [degrees]	
0 -10	0
> 10	0

R. m. s. d. and restraint figures in parentheses are the results of similar calculations performed only with constraints that could be obtained from 600 and 750 MHz spectra. Information obtained from the 900 MHz data was excluded from these calculations.

 $[^]a$ The N-terminal NH3 $^+$, Pro N-atoms and carbonyl C′-atoms before Pro residues were not considered to calculate the fraction.

 $[^]b$ Lys NH3⁺, Arg NH2, side chain carbonyl and aromatic C $^\gamma$ -carbons were not considered to calculate the fraction.

^cRelative to pairs with non-degenerate chemical shifts.

dIncludes 14 residues: Trp 19, Trp 26, Ala 45, Val 54, Val 56, Ala 73, Pro 75, Ile 84, Thr 97, Val 101, Thr 104, Ile 110, Ser 114, and Leu 131 which were located in the binding cavity and had heavy side chain atom displacements < 0.9 Å after superposition of the backbone atoms of regular secondary structure elements for minimal r. m. s. d.